UNIVERSITY OF CALIFORNIA SAN DIEGO

Mitigation of Resistive Drift Wave and Ion Temperature Gradient Instabilities by Velocity Shear

A Thesis submitted in partial satisfaction of the requirements
for the degree Master of Science

in

Engineering Sciences (Engineering Physics)

by

Yevgeniy Yakusevich

Committee in charge:

Professor Sergei Krasheninnikov, Chair
Professor Alexey Arefiev
Professor Oliver Schmidt

2023

The Thesis of Yevgeniy Yakusevich is approved, and it is acceptable in quality and form for publication on microfilm and electronically.

University of California San Diego

2023

TABLE OF CONTENTS

LIST OF FIGURES

LIST OF ABBREVIATIONS

RT	Rayleigh-Taylor
IM	Interchange Mode
RDW	Resistive Drift Wave
ITG	Ion Temperature Gradient

LIST OF SYMBOLS

V_0'	Velocity Shear
γ	Growth Rate of the Instability
$n, \bar{n}, \Delta n$	Plasma Density, Mean Plasma Density, Plasma Density Difference
$T_i, \bar{T}_i, \Delta T_i$	Ion Temperature, Mean Ion Temperature, Ion Temperature Difference
W	Characteristic Width of the Plasma Density/Ion Temperature Profiles
n_e	Electron Density
T_e	Electron Temperature
e	Electron Charge
k_x, k_y, k_z	X (Radial), Y (Poloidal), and Z (Toroidal) Wavenumbers of the Instability
ω	Frequency of the Instability
ξ	X (Radial) Coordinate, Renormalized by W
κ_x, κ	X (Radial) and Y (Poloidal) Wavenumbers, Renormalized by W
ϕ	Electrostatic Potential
ω_*	Drift Wave Base Frequency
c_s	Plasma Speed of Sound
ρ_i	Ion Gyroradius

ρ_s	"Effective Gyroradius" for Cold Ions
$\nu_{\parallel}$	Characteristic Rate of Electron Diffusion Parallel to the Magnetic Field
v_{Te}, v_{Ti}	Electron and Ion Thermal Velocities
ν_{ei}	Electron-Ion Collision Frequency
L_n, L_B	RDW Density Gradient and ITG Magnetic Field Gradient Scale Lengths
Ω_{Bi}	Ion Gyrofrequency
M	Ion Mass

ACKNOWLEDGEMENTS

I would like to acknowledge Professor Sergei Krasheninnikov for his support as the chair of my committee and my principal investigator. Through multiple drafts and revisions, his guidance has proved to be vital to the completion of this thesis. Professor Sergei Krasheninnikov composed much of the introductory paragraphs of this work, with modest stylistic adjustments by the dissertation author.

This work was supported by the U.S. Department of Energy, Office of Science, Office of Fusion Energy Sciences under Award No. DE-FG02-04ER54739 at UCSD.

The abstract, body text, and figures of this work have also been submitted for publication of the material as it may appear in Physics of Plasmas, 2023. Yakusevich, Yevgeniy; Krasheninnikov, Sergei, AIP Publishing, 2023. The thesis author was the primary investigator and author of this paper.

VITA

2019 Bachelor of Science in Physics, University of California Santa Barbara

2020 Student Research Intern, Princeton Plasma Physics Laboratory

2023 Master of Science in Engineering Sciences (Engineering Physics), University of California San Diego

PUBLICATIONS

"Correction and Verification of X-Ray Imaging Crystal Spectrometer Analysis on Wendelstein 7-X through X-Ray Ray Tracing"
Review of Scientific Instruments, vol. 92, 043530 (2021); DOI:10.1063/5.0043513

"Design and Expected Performance of a Variable-Radii Sinusoidal Spiral X-Ray Spectrometer for the National Ignition Facility"
Review of Scientific Instruments, vol. 92, 093904 (2021); DOI:10.1063/5.0054329

"Resonant Three-Wave Interactions with Linear Source/Sink Terms: Exploring the Parameter Space"
Physics of Plasmas, Vol. 29, 080701 (2022); DOI:10.1063/5.0098271

FIELD OF STUDY

Major Field: Engineering Physics
Studies in Applied Plasma Physics
Professor Sergei Krasheninnikov

ABSTRACT OF THE THESIS

Mitigation of Resistive Drift Wave and Ion Temperature Gradient Instabilities by Velocity Shear

by

Yevgeniy Yakusevich

Master of Science in Engineering Sciences (Engineering Physics)

University of California San Diego, 2023

Professor Sergei Krasheninnikov, Chair

The effects of velocity shear on the resistive drift wave instability in the non-adiabatic limit and the toroidal ion temperature gradient instability are investigated for a plasma of inhomogeneous density/ion temperature, respectively. For the resistive drift wave, we find that the instability growth rate decreases monotonically with increasing magnitude of shear, but we find that complete stabilization is impossible. For the ion temperature gradient instability, we find that the standard WKB approximation is insufficient to describe the full behavior of the instability, and that an analysis of the localized eigenmode problem reveals two separate

unstable solutions which the WKB approximation does not predict. The impact of flow shear on these two new unstable solutions is discussed. In both resistive drift wave and ion temperature gradient instabilities, the sheared flow causes a shifting, tilting, and sharpening of the electrostatic potential eddies.

INTRODUCTION

It is widely accepted that the shear of plasma flow alters plasma instabilities and can result in the improvement of plasma confinement in magnetic fusion devices (see Refs. [1] [2] [3] [4] and the references therein). In this regard, a simple "quench rule" is often used for the assessment of the impact of plasma flow shear [4] [5] [6], stating that the instability is "stabilized" when the velocity shear $|V_0'|$ exceeds the instability growth rate γ. This rule goes back to the foundational studies of the impact of fluid flow on instabilities in stratified fluids [7] [8] [9]. However, recent results [10] undoubtedly demonstrate that, whereas the quench rule $|V_0'| \geq \gamma$ could be applied to the Rayleigh-Taylor (RT) and interchange mode (IM) plasma instabilities, it fails to describe the stabilization of the resistive drift wave (RDW) instability in the adiabatic limit even for $|V_0'| \gg \gamma$. The reason for such a difference is the virtually irreversible charge separation which drives the IM, contrasted with the almost fully reversible charge separation driving the RDW instability in the adiabatic limit [10]. Thus, the quench rule is insufficient to describe the shear-response of every plasma instability, and it is important to have a thorough understanding of the impact of plasma velocity shear on other instabilities playing important roles in anomalous plasma transport. Therefore, in this work, we consider the impact of constant plasma velocity shear on the RDW instability in non-adiabatic limit [4] in Chapter 1, then on the toroidal ion temperature gradient (ITG) instability [11] in Chapter 2; we then summarize and discuss the results of our studies in the conclusion.

For both RDW and ITG modes we will use the slab approximation with "x" and "y" to be analogous to radial and poloidal coordinates, respectively. We will analyze the impact of velocity shear on the "standing" RDW and ITG modes and consider some particular density profile $n(x)$ for the RDW and ion temperature profile $T_i(x)$ for the ITG:

$$n(x) = \bar{n} - \Delta n \tanh(x/\mathrm{W})\,/2, \quad (1)$$

$$T_i(x) = T_i - \Delta T \,\mathrm{atan}(x/W)\,/\pi, \quad (2)$$

where W is the characteristic width of the profile variation. In what follows we assume $\Delta n \ll \bar{n}$ and $\Delta T \ll T_i$. These profiles allow analytic solutions for their corresponding eigenfunction/eigenvalue equations for the case of no velocity shear. For simplicity, we consider all other parameters involved (e.g., electron temperature, T_e, for the RDW and ITG modes and electron density, n_e, for the ITG mode) to be constant. In addition, we adopt the Boussinesq approximation. To avoid the possible impact of the Kelvin-Helmholtz instability, we consider a constant shear of the y-component of plasma velocity: $V_0' = dV_0/dx = const$. Since our setup of the linear stability problem is homogeneous in the y-direction and in time, we use the Fourier decomposition in the y-coordinate and in time, thereby introducing the wave number k_y and the frequency ω.

Acknowledgements

Professor Sergei Krasheninnikov composed much of the introductory paragraphs of this work, with modest stylistic adjustments by the dissertation author.

Chapter 1 – Resistive Drift Wave Instability in the Non-Adiabatic Limit

For the RDW instability we adopt the cold ion limit and constant electron temperature approximation, introduce dimensionless variables and renormalizations $\xi = x/W$, $\kappa = \mathrm{W}k_y$, $e\phi/T_e \to \phi$, $\omega L_n/c_s \to \omega$, $V_0' L_n/c_s \to V_0'$ and use the quasi-neutrality condition and the relation between electron density and electrostatic potential perturbations from [12] in the limit of non-adiabatic electrons $\nu_\parallel \ll \omega_*$; here, $\omega_* = k_y c_s \rho_s / L_n$ is the drift wave base frequency, $\nu_\parallel = v_{Te}^2 k_z^2 / \nu_{ei}$ is the characteristic rate for an electron to diffuse a parallel wavelength $\sim k_z^{-1}$, v_{Te} is the electron thermal velocity, ν_{ei} is the electron-ion collision frequency, $L_n = 2\mathrm{W}\bar{n}/\Delta n$ is the plasma density gradient scale length, $c_s = \sqrt{T_e/M}$ is the plasma sound speed, $\rho_s = c_s/\Omega_{Bi}$ is the effective cold ion gyroradius, M is the ion mass, and Ω_{Bi} is the ion gyrofrequency. With these, we arrive at the following eigenfunction/eigenvalue equation (see also Eq. (VII.34) from Ref. [13]):

$$\frac{d^2\phi}{d\xi^2} - \kappa^2\phi + i\frac{\Omega_{Bi}\nu_\parallel}{\tilde{\omega}^2}\frac{W\kappa}{L_n}\frac{1}{\cosh^2(\xi)}\phi = 0, \tag{3}$$

where $\tilde{\omega} \equiv \omega - \kappa V_0' \xi$.

Comparing Eq. (3) with the similar equation (2) from Ref. [10] for the Rayleigh-Taylor (RT) instability, we find that, with a proper re-normalization, they are identical; thus, we can use the analytic results from Ref. [10]. For the case of no velocity shear, we use the similarity of Eq. (3) with the Schrödinger equation [14], which is characterized by the quantum integer number m; the most unstable solution corresponds to $m = 0$, which yields the following eigenfunction/eigenvalue pair:

$$\phi_0(\xi) = \cosh^{-|\kappa|}(\xi), \qquad \omega_0^2 = \frac{i}{2}\frac{\Delta n}{\bar{n}}\frac{|\kappa|}{\kappa^2+|\kappa|}\Omega_{Bi}\nu_\parallel, \tag{4}$$

To investigate the effect of shear, we follow Ref. [10] and employ the method of successive approximation to the solution of Eq. (3) by expanding both ω and ϕ in powers of V_0': $\omega = \sum_j \omega_j V_0'^j$, $\phi = \sum_j \phi_j V_0'^j$, and using the integral relation following from Eq. (3):

$$\int_{-\infty}^{\infty}\left(-\left|\frac{d\phi}{d\xi}\right|^2 - \kappa^2|\phi|^2 + \frac{\kappa^2+|\kappa|}{\cosh^2(\xi)}|\phi|^2\right)d\xi = \int_{-\infty}^{\infty}\left(1-\frac{\omega_0^2}{\tilde{\omega}^2}\right)\frac{\kappa^2+|\kappa|}{\cosh^2(\xi)}|\phi|^2 d\xi\,, \qquad (5)$$

We note that the left-hand-side of Eq. 5 must be real, while the right-hand-side contains both imaginary-valued ω_0^2 and complex-valued ω, therefore the only way for the integral relation to be satisfied is $\mathrm{Im}(\omega) \neq 0$, which indicates that the instability can never be fully stabilized by shear. Based on the results from Ref. [10] on an impact of velocity shear on the RT instability, this approach works rather well for small magnitude of V_0'. Following Ref. [10], we perform the successive approximation to second order of V_0', as the first order does not yield any correction to the instability growth rate, to obtain the following expansion coefficients:

$$\omega_1 = 0\,, \qquad \omega_2 = \omega_0^* \frac{(V_0'\kappa)^2}{|\omega_0|^2}\left[2(\kappa^2+|\kappa|)\frac{I(|\kappa|)}{I_0(|\kappa|)} + \frac{3}{2}\frac{I_2(|\kappa|)}{I_0(|\kappa|)}\right], \qquad (6)$$

where the integrals are

$$I_0(|\kappa|) = \int_{-\infty}^{\infty}\frac{1}{\cosh^{2|\kappa|+2}(\xi)}d\xi, \qquad I_2(|\kappa|) = \int_{-\infty}^{\infty}\frac{\xi^2}{\cosh^{2|\kappa|+2}(\xi)}d\xi,$$

$$I(|\kappa|) = \int_{-\infty}^{\infty}\frac{\xi d\xi}{\cosh^{2|\kappa|+2}(\xi)}\int_0^{\xi}\cosh^{2|\kappa|}(\xi')\,d\xi'\int_{\xi'}^{\infty}\frac{\xi'' d\xi''}{\cosh^{2|\kappa|+2}(\xi'')},$$

and ω_0^* is the complex-conjugate of ω_0. Since all integrals involved in Eq. (6) are positive [10], the imaginary part of ω_2 is guaranteed to be negative, and so this analytical model shows a general downward trend in the instability growth rate with increasing $|V_0'|$ and provides the following asymptotic expressions:

$$\omega_2|_{|\kappa|\to\infty} = \omega_0^*\frac{(V_0'\kappa)^2}{2|\omega_0|^2}, \qquad \omega_2|_{|\kappa|\to 0} = \omega_0^*\frac{\pi^2}{8}\frac{(V_0'\kappa)^2}{|\omega_0|^2}, \qquad (7)$$

Since the method of successive approximation is only valid for small shear, a direct numerical solution is necessary to deduce if this trend persists. Thus, in addition to the method of successive approximation, we also solved for the growth rate $\Gamma = \mathrm{Im}(\omega)/\mathrm{Im}(\omega_0)$ numerically using MATLAB: we discretized Eq. (2) using 4th order central difference [15], converted it into a quadratic eigenvalue problem, then solved using a Krylov-Schur decomposition algorithm to find the most unstable eigenmodes. We find that, for the RDW, the growth rate of the instability decreases monotonically with increasing shear, and that the analytical approximation is mostly accurate but slightly underestimates the growth rate at large shear and $|\kappa| \lesssim 1$ (Figure 1.1). We also find that increasing shear causes shifting, tilting, and sharpening of the eddies of the electrostatic potential ϕ (Figure 1.2).

For perspective, we estimate a value of the normalized shear V_0' from 0.2 to 2 for most tokamaks [16] [17], as well as $\kappa \sim 0.05$ and $\mathrm{Im}(\omega_0) \sim 100$. This level of shear is three to four orders of magnitude too little to have a meaningful impact on the RDW instability.

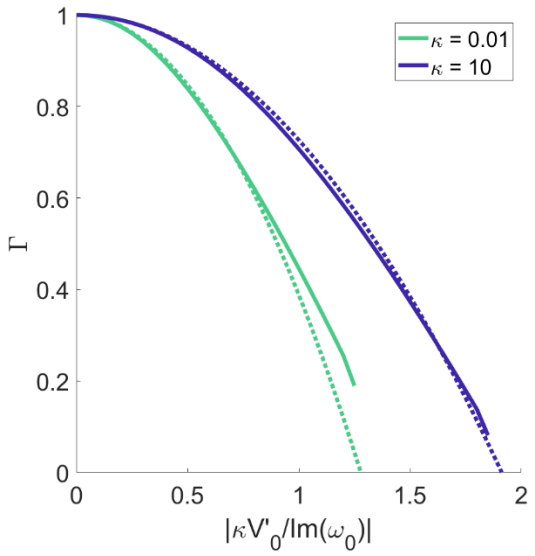

Figure 1.1: Plot of the RDW instability growth rate at two values of κ (solid lines) and analytical predictions thereof (dashed lines), showing monotonic stabilization with $|V_0'|$.

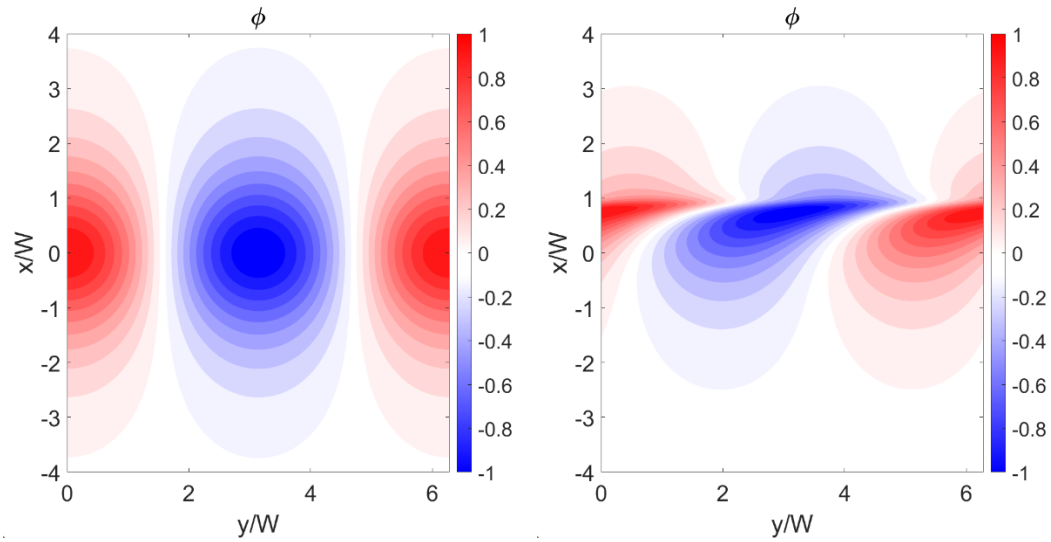

Figure 1.2: Contours of the RDW electrostatic potential eigenfunction $\phi(\xi)$ for $\kappa = 1$ comparing the cases of $\kappa V_0'/\mathrm{Im}(\omega_0) = 0$ (left) and 1.5 (right), showing a shifting, tilting, and sharpening of the potential.

Chapter 2 – Toroidal Ion Temperature Gradient Instability

For the ITG instability, we start from the electrostatic ion gyrokinetic equations 2.9 and 2.10 in Ref. [18], assume constant electron temperature and density, then neglect nonlinear cross-terms in Poisson brackets, any collision terms, and the first term in the expansion of the gyroaveraging operator assuming that $\rho_i k_y \leq \sqrt{T_e/T_i} \sim \mathcal{O}(1)$, where $\rho_i = v_{Ti}/\Omega_{Bi}$ is the ion gyroradius. We introduce dimensionless variables and renormalizations $\xi = x/W$, $\kappa = Wk_y$, $e\phi/T_e \rightarrow \phi$, $\omega L_B/2c_s \rightarrow \omega$, $V_0' L_B/2c_s \rightarrow V_0'$, where $1/L_B = -\mathrm{d}\ln B\,/dx$ is the magnetic field gradient scale length. This leads to the following eigenfunction/eigenvalue equation, as well as dimensionless parameters α (which represents the ion temperature gradient), and $W_\rho = W/\rho_s$:

$$\frac{\partial^2\phi}{\partial\xi^2} - W_\rho^2\left[\frac{\widehat{\omega}+1}{\alpha(\xi)} + \frac{1}{\widehat{\omega}} + \frac{\kappa^2}{W_\rho^2}\right]\phi = 0, \tag{8}$$

$$\alpha(\xi) = \frac{\Delta T}{T_e}\frac{L_B}{2\pi W}\frac{1}{1+\xi^2} \equiv \frac{\alpha_0}{1+\xi^2}\,, \tag{9}$$

Here, $\widehat{\omega} = \Omega - W_\rho V_0'\xi$ and $\Omega \equiv W_\rho\omega/\kappa$. We estimate α_0 to be on the order of 10 to 100 for most tokamaks and will only consider the limit of large α_0.

Applying the WKB approximation (see ref. [18]) reduces the second derivative term in Eq. (8) to $-\kappa_x^2\phi$ and allows us to take $\alpha(\xi) \approx \alpha_0$ as locally constant. Thus, for the case of zero shear, Eq. (8) reduces to:

$$\frac{\Omega+1}{\alpha_0} + \frac{1}{\Omega} + \frac{\kappa_x^2}{W_\rho^2} + \frac{\kappa^2}{W_\rho^2} = 0, \qquad \Omega = \frac{W_\rho^2+\alpha_0(\kappa_x^2+\kappa^2)}{2W_\rho^2}\left[-1 \pm \sqrt{1 - 4\alpha_0\left(\frac{W_\rho^2}{W_\rho^2+\alpha_0(\kappa_x^2+\kappa^2)}\right)^2}\right], \tag{10}$$

This WKB solution for ω indicates that, in the limit of large α_0, there exists a critical wavenumber $\kappa_*^2 \equiv 2W_\rho^2/\sqrt{\alpha_0}$ such that $0 < \kappa_x^2 + \kappa^2 < \kappa_*^2$ leads to unstable solutions. On the other hand, for the case of $\kappa^2 > \kappa_*^2$, we instead obtain two stable solutions:

$$\Omega \approx -\alpha_0/\left(1+\alpha_0(\kappa_x^2+\kappa^2)/W_\rho^2\right), \tag{11}$$

$$\Omega \approx -1-\alpha_0(\kappa_x^2+\kappa^2)/W_\rho^2, \tag{12}$$

The WKB approximation works under the condition that the ion temperature gradient does not change too quickly over the span of a wavelength W/κ_x, such that $\alpha(\xi)$ can be considered locally constant. This is encapsulated in the condition that $\kappa_x \gg 1$; if this is not true, then the result given by the WKB approximation is inaccurate.

A more accurate solution eschews the WKB approximation and solves the governing equation (8) directly. For the case of zero shear, we note the similarity between Eq. (8) and Weber's equation [19], which has solutions in the form of the parabolic cylinder functions [20]:

$$\phi(\xi) = 2^{-m/2}\exp(-\xi^2/4\beta^2)\,H_m\left(\xi/\sqrt{2}\beta\right), \tag{13}$$

$$\frac{\Omega+1}{\alpha_0}+\frac{1}{\Omega}+\frac{\kappa^2}{W_\rho^2} = \pm\frac{2m+1}{W_\rho}\sqrt{\frac{\Omega+1}{\alpha_0}}, \tag{14}$$

where $H_m(\xi)$ is the Hermite polynomial, $\beta = \pm\sqrt{\alpha_0/(\Omega+1)}/2W_\rho$ such that $\mathrm{Re}(\beta) > 0$, and $m = 0,1,2,\ldots$ is the eigenmode number.

The term on the right-hand side of Eq. 14 resembles the κ_x^2 term in Eq. 10, but due to it containing Ω, it is capable of taking on complex values and varying with κ, thus altering the stability properties of the system. The previously stable solution Eq. 11 becomes the "local solution" and is now unstable for $\kappa_* < \kappa \leq W_\rho$, as seen in Figure 2.1. Likewise, Eq. 12 becomes the "global solution" and is now unstable everywhere, as seen in Figure 2.2. We find that the destabilization of the local solution makes little qualitative difference compared to WKB, whereas the destabilization of the global solution is significantly different from WKB and warrants closer examination. To illustrate the behavior of the global solution, we perform a three-term dominant

balance on Eq. 14 to eliminate the $1/\Omega$ term; this is possible when $\kappa \gtrsim \kappa_*$, and yields the following solution:

$$\Omega = \alpha_0\left(-\kappa^2 + 2\kappa_m^2 \pm 2i\kappa_m\sqrt{\kappa^2 - \kappa_m^2}\right)/W_\rho^2 - 1, \quad \kappa_m = m + 1/2, \tag{15}$$

Here, it is important to note that the higher eigenmodes of the global solution are initially stable, but each destabilize at a critical point κ_m that is analogous to κ_x from WKB, and each mode grows $\mathrm{Im}(\omega) \propto \kappa_m\kappa^2$ until it is more unstable than all lower eigenmodes below it. Eq. 15 predicts that, for large $\kappa > \kappa_*$, the overall instability growth rate out of all eigenmodes scales with $\mathrm{Im}(\omega) \sim \alpha_0\kappa^3/W_\rho^3$ (Figure 2.2).

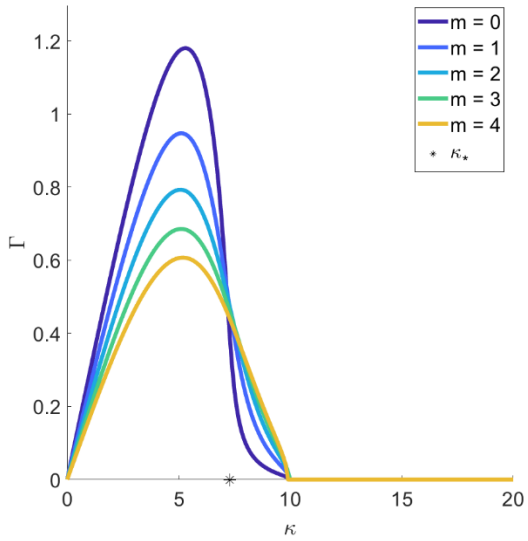

Figure 2.1: Analytic predictions ($\alpha_0 = 10, W_\rho = 10$) of the no-shear instability growth rate for the first few modes of the local solution, as well as k_*. Note the peak instability at $\kappa_{max} = 5.3$, $\Gamma_{max} = 1.18$, the complete stabilization of the instability at $\kappa = W_\rho$, and the higher eigenmodes overtaking the lower ones at $\kappa_* < \kappa < W_\rho$.

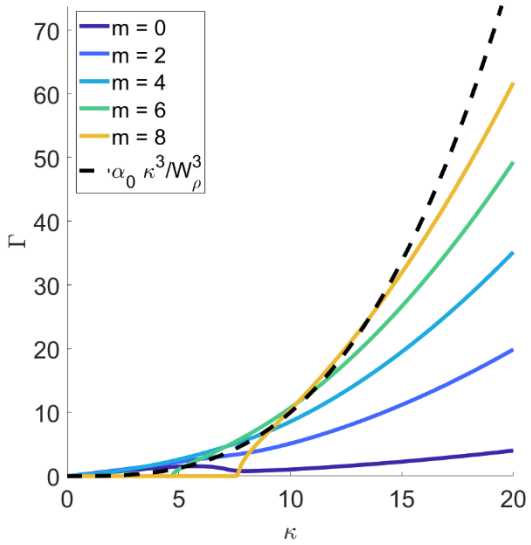

Figure 2.2: Analytic predictions ($\alpha_0 = 10, W_\rho = 10$) of the no-shear instability growth rate for the first few modes of the global solution. Note the higher eigenmodes growing more unstable than the lower ones and overtaking them constantly. The dashed line represents a prediction of the largest Γ out of all modes.

Having obtained the analytical solutions for the case of no shear, we then solved for the shear response of the growth rate $\Gamma = \mathrm{Im}(\omega)$ numerically using MATLAB. We discretized Eq. (8) using 4th order central difference [15], converted it into a quadratic eigenvalue problem, then solved using a Krylov-Schur decomposition algorithm to find the most unstable eigenmodes. We then investigated the shear response of both the local and global solutions over a range of parameters α_0 and W_ρ both from 1 to 100.

For the local solution, we find that each combination of parameters α_0 & W_ρ yields a curve of growth rates $\Gamma(\kappa, V_0')$ with a maximal value Γ_{max} at a wavenumber $\kappa_{max} < \kappa_*$ and $V_0' = 0$, such as Fig. 3a. We only consider the shear response of the local ITG at $\kappa = \kappa_{max}$, and find that increasing $|V_0'|$ causes the growth rate of all eigenmodes to decrease monotonically (Figure 2.3), until the 0th and most unstable eigenmode is quenched at a critical value V'_{quench}.

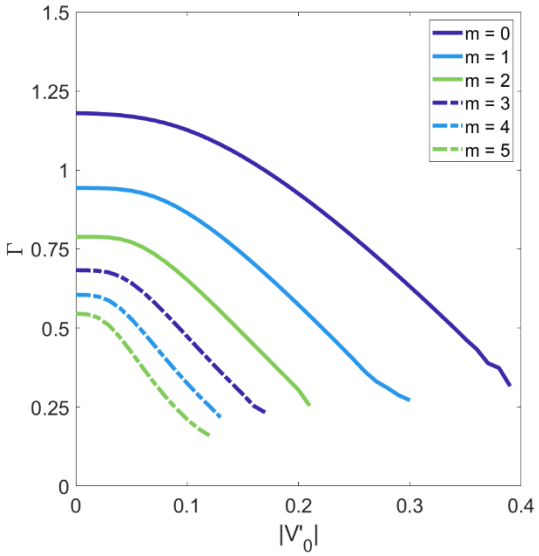

Figure 2.3: Plot of the ITG local solution's first 6 eigenmodes ($\alpha_0 = 10, W_\rho = 10, \kappa = 5.3$) over $|V_0'|$, showing monotonic shear-induced stabilization of all eigenmodes.

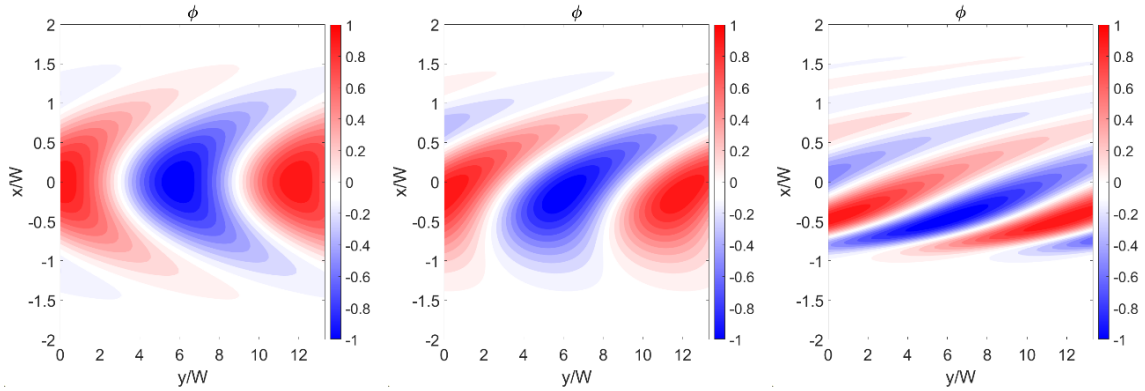

Figure 2.4: Contours of the electrostatic potential of the ITG local solution's 0th eigenfunction $\phi_0(\xi)$ ($\alpha_0 = 10, W_\rho = 10, \kappa = 5.3$) comparing the cases of $V_0' = 0$ (left), 0.1 (center), and 0.4 (right).

For the global solution, Eq. 15 indicates that the instability growth rate grows monotonically $\propto \kappa^3$, and thus κ_{max} does not exist (Figure 2.2), which necessitates that we additionally scan over κ from 0 to $2W_\rho$. We find that increasing $|V_0'|$ initially destabilizes the global solution, leading to the 0th eigenmode overtaking all of the others and becoming the most unstable (Figure 2.5). However, the effect of shear is not monotonically destabilizing, and we find that each combination of parameters $\alpha_0, W_\rho, \& \kappa$ yields a curve of growth rates $\Gamma(V_0')$ with a

maximal value Γ_{max} at a shear V'_{max}, after which any further shearing decreases the growth rate until it is quenched at a critical value V'_{quench} (Figure 2.7). In both cases, we find that shear causes shifting, tilting, and sharpening of the eigenfunction as well as an increase in the "effective" eigenmode number (Figure 2.4 & Figure 2.6).

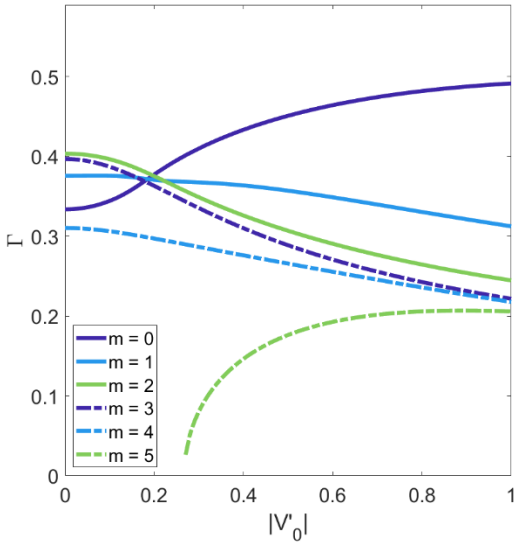

Figure 2.5: Plot of the ITG global solution's first 6 eigenmodes ($\alpha_0 = 10, R_W = 10, \kappa = 1$) over $|V'_0|$, showing the 0th eigenmode overtaking the others as the most unstable.

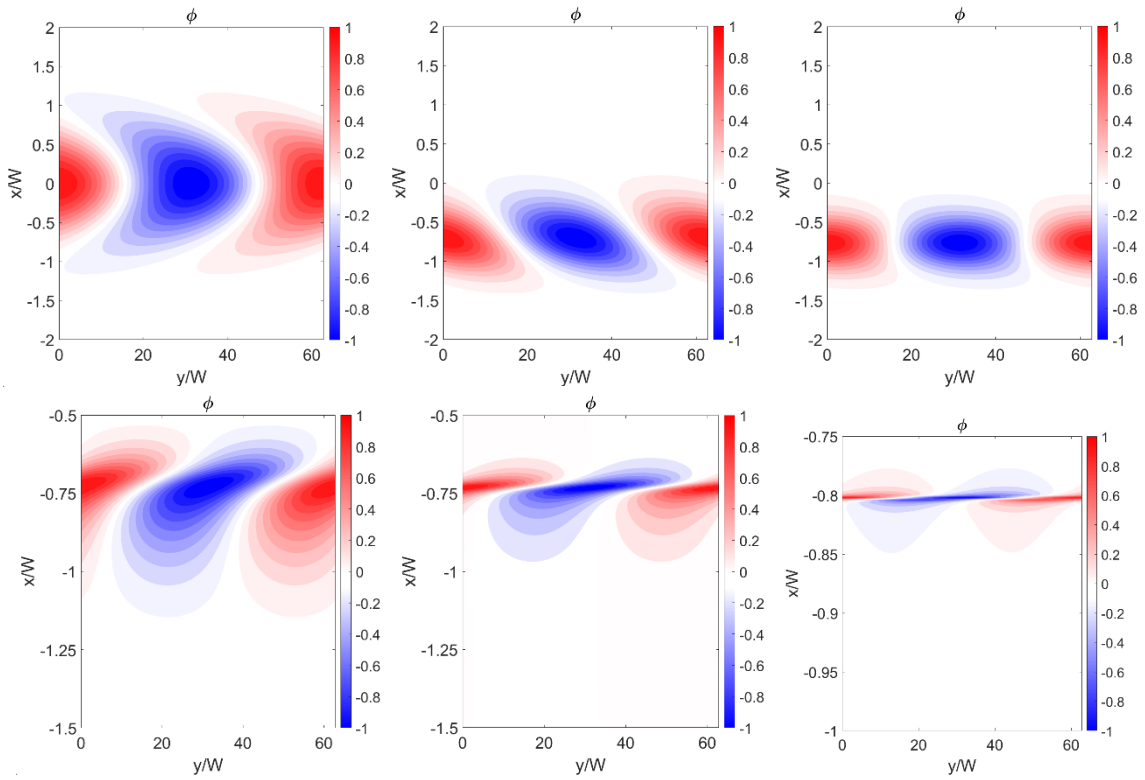

Figure 2.6: Contours of the electrostatic potential of the ITG global solution's 0^{th} eigenfunction $\phi_0(\xi)$ $(\alpha_0 = 10, W_\rho = 10, \kappa = 1)$ comparing the cases of $V_0' = 0, 0.5, 1, 5, 10, 50$ (top left to bottom right).

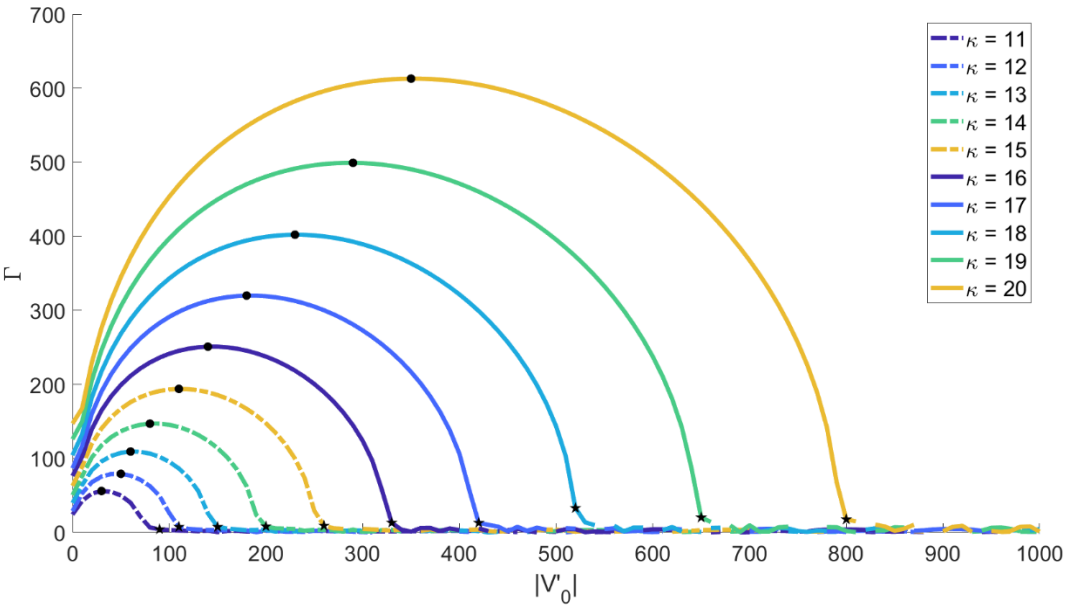

Figure 2.7: Results for shear stabilization of the ITG global solution ($\alpha_0 = 10, W_\rho = 10$) with 10 values of κ. Dots indicate instability growth rate maxima at (V'_{max}, Γ_{max}), while stars indicate shear-induced quenching of the instability at V'_{quench}.

We compare our results to the nonlinear simulation results obtained in Ref. [18], which concludes suppression and stabilization of the ITG instability at levels of shear consistent with the quench rule $V'_{quench} \approx 2\Gamma_{max}$ for α_0 from 0.16 to 7.29 and arbitrary W_ρ. For the local solution, we find that the quench rule is better described as a parabola $W_\rho V'_{quench} \approx 2.50\Gamma^2_{max} + 1.45\Gamma_{max}$ (Figure 2.8), whereas for the global solution, we find results consistent with the quench rule $V'_{quench} \approx 1.36\ \Gamma_{max}$ (Figure 2.9). We also find the following relationships in the global solution: $V'_{quench} \approx 2.32\ V_{max}$ (Figure 2.10) and $V'_{quench} \approx 0.5\ \alpha_0 \kappa^4 / W_\rho^3$ (Figure 2.11).

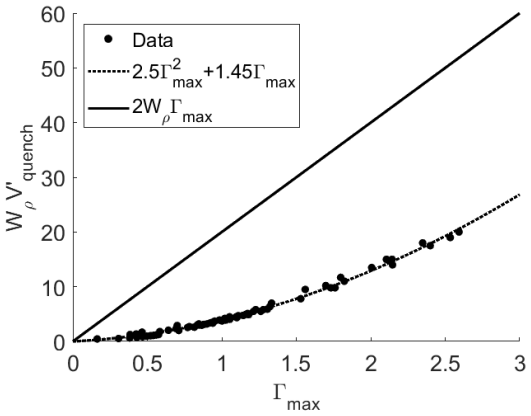

Figure 2.8: Plot of shear $W_\rho V'_{quench}$ vs. Γ_{max} for the ITG local solution, with quadratic fit (dashed line) compared to the results from Fig. 12 of Ref. [18] (solid line) assuming $W_\rho = 10$

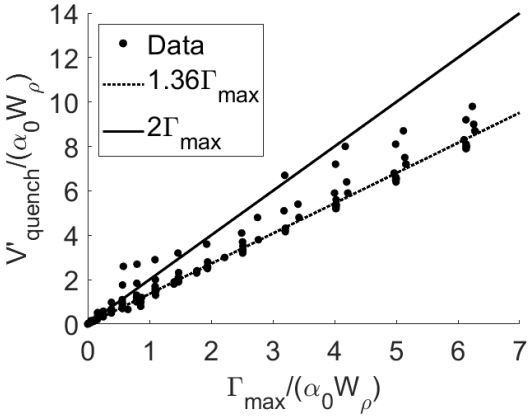

Figure 2.9: Plot of V'_{quench} vs. Γ_{max} for the ITG global solution, with linear fit (dashed line) compared to the results from Fig. 12 of Ref. [18] (solid line)

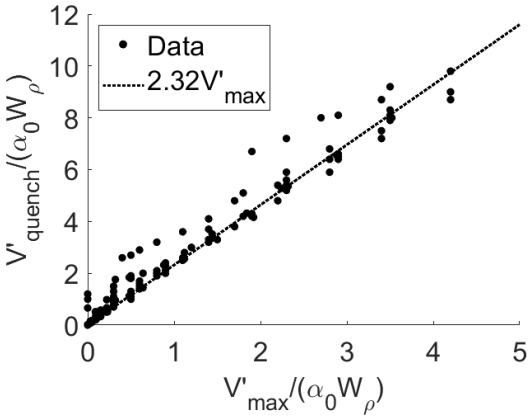

Figure 2.10: Plot of V'_{quench} vs. V'_{max} for the ITG global solution, with linear fit.

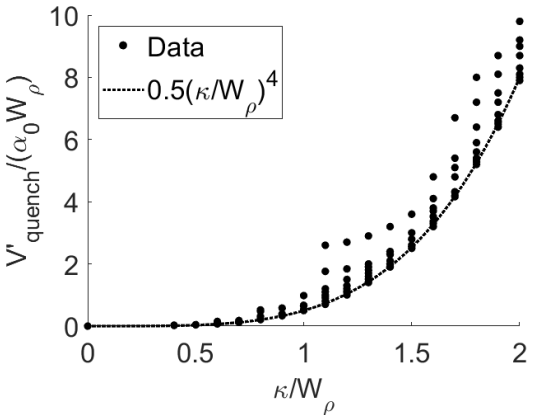

Figure 2.11: Plot of V'_{quench} vs. κ for the ITG global solution, with quartic fit.

For perspective, we estimate a value of the normalized shear V'_0 from 1 to 10 for most tokamaks [16] [17], as well as $W_\rho \sim 100$ and α_0 from 10 to 100. This level of shear is enough to suppress all local ITG instabilities, but two to three orders of magnitude too little to suppress any of the global ITG instabilities, thus rendering the toroidal ITG instability practically unquenchable.

CONCLUSION

In conclusion, we investigated the effect of a constant velocity flow shear on both the non-adiabatic RDW and toroidal ITG instabilities using both analytical and numerical methods.

For the RDW, we obtain an analytical model that predicts the behavior of the instability for small shear but also concludes that the instability cannot be completely quenched. With the aid of numerical modeling, we find that the analytical model is mostly accurate for larger shear but somewhat underestimates γ for small $|\kappa| \lesssim 1$. We also find that the shear necessary to attenuate all non-adiabatic RDW instabilities, $V_0' \geq 2\mathrm{Im}(\omega_0)/\kappa$, does not abide by the quench rule.

For the ITG, we found that the standard WKB approximation is insufficient as an analytical model, and that direct solution of the governing differential equation shows more instability than the WKB approximation predicts. Of the two solutions predicted by our Weber analytical model, the global solution is consistently more unstable than the local solution and is initially destabilized by shear before peaking at V'_{max} and stabilizing at a higher shear $V'_{quench} \geq 1.36\ \Gamma_{max}$.

Acknowledgements

The abstract, body text, and figures of this work have also been submitted for publication of the material as it may appear in Physics of Plasmas, 2023. Yakusevich, Yevgeniy; Krasheninnikov, Sergei, AIP Publishing, 2023. The thesis author was the primary investigator and author of this paper.

REFERENCES

[1] W. Horton, "Drift waves and transport," *Rev. Mod. Phys.,* vol. 71, no. 3, pp. 735-778, Apr 1998.

[2] R. Groebner, K. Burrell and R. Seraydarian, "Role of edge electric field and poloidal rotation in the L-H transition," *Phys. Rev. Lett.,* vol. 65, p. 3015, 1990.

[3] P. H. Diamond, S. Itoh, K. Itoh and T. Hahm, "Zonal flows in plasma – A review," *Plasma Phys. Contr. Fusion,* vol. R35, p. 47, 2005.

[4] W. Horton, Turbulent Transport in Magnetized Plasmas, 2nd ed., World Scientific, 2018.

[5] R.Waltz, G. Staebler, W. Dorland, G. Hammett, M. Kotschenreuther and J. Konings, "A gyro-landau-fluid transport model," *Phys. Plasmas,* vol. 4, p. 2482–2496, 1997.

[6] J. Kinsey, R. Waltz and J. Candy, "Nonlinear gyrokinetic turbulence simulations of E X B shear quenching of transport," *Phys. Plasmas,* vol. 12, p. 062302, 2005.

[7] L. Kelvin, "Stability of fluid motion: Rectilinear motion of viscous fluid between two parallel plates," *Philos. Mag.,* vol. 24, p. 188–196, 1887.

[8] H. Kuo, "Perturbations of plane Couette flow in stratified fluid and origin of cloud streets," *Phys. Fluids,* vol. 6, p. 195–211, 1963.

[9] S. Chandrasekhar, Hydrodynamic and Hydromagnetic Stability, Courier Corporation, 2013.

[10] Y. Zhang, S. I. Krasheninnikov and A. I. Smolyakov, "Different responses of the Rayleigh–Taylor type and resistive drift wave instabilities to the velocity shear," *Physics of Plasmas,* vol. 27, p. 020701, 2020.

[11] P. N. Guzdar, L. Chen, W. M. Tang and P. H. Rutherford, "Ion-temperature-gradient instability in toroidal plasmas," *Physics of Fluids,* vol. 26, no. 3, p. 673–677, 1 March 1983.

[12] J. R. Angus and S. I. Krasheninnikov, "Drift wave dispersion relation for arbitrarily collisional plasma," *Physics of Plasmas,* vol. 19, p. 052504, 2012.

[13] S. Krasheninnikov, A. Smolyakov and A. Kukushkin, On the Edge of Magnetic Fusion Devices, Springer Series in Plasma Science and Technology, 2007.

[14] L. Landau and E. Lifshitz, Quantum Mechanics: Non-Relativistic Theory, vol. 3, Elsevier, 2013.

[15] C. R. Taylor, "Finite Difference Coefficients Calculator," 2016. [Online]. Available: https://web.media.mit.edu/~crtaylor/calculator.html. [Accessed 2023].

[16] L. Schmitz, L. Zeng, T. L. Rhodes, J. C. Hillesheim, W. A. Peebles, R. J. Groebner, K. H. Burrell, G. R. McKee, Z. Yan, G. R. Tynan, P. H. Diamond, J. A. Boedo, E. J. Doyle, B. A. Grierson, C. Chrystal, M. E. Austin, W. M. Solomon and G. Wang, "The role of zonal flows and predator–prey oscillations in triggering the formation of edge and core transport barriers," *Nuclear Fusion*, vol. 54, p. 073012, 2014.

[17] L. Schmitz, L. Zeng, T. L. Rhodes, J. C. Hillesheim, E. J. Doyle, R. J. Groebner, W. A. Peebles, K. H. Burrell and G. Wang, "Role of Zonal Flow Predator-Prey Oscillations in Triggering the Transition to H-Mode Confinement," *Phys. Rev. Lett.*, vol. 108, p. 155002, 2012.

[18] P. G. Ivanov, A. A. Schekochihin, W. Dorland, A. R. Field and F. I. Parra, "Zonally dominated dynamics and Dimits threshold in curvature-driven ITG turbulence," *Journal of Plasma Physics*, vol. 86, p. 855860502, 2020.

[19] D. Zwillinger, Handbook of Differential Equations, 3rd ed., Boston: Academic Press, 1997, p. 128.

[20] I. S. Gradshteyn and I. M. Ryzhik, Table of Integrals, Series, and Products, Sixth ed., San Diego: Academic Press, 2000.